ELSEVIER

Catalysis Today 78 (2003) 91–104

CATALYSIS TODAY

www.elsevier.com/locate/cattod

Solid-state ^{51}V NMR for characterization of vanadium-containing systems

O.B. Lapina [a,*], A.A. Shubin [a], D.F. Khabibulin [a], V.V. Terskikh [a], P.R. Bodart [b], J.-P. Amoureux [b]

[a] *Boreskov Institute of Catalysis, Prosp. Lavrentieva 5, 630090 Novosibirsk, Russia*
[b] *Laboratoire de Dynamique et Structure des Matériaux Moléculaire, Universite des Sciences et Technologies de Lille, F-59655 Villeneuve d'Ascq, France*

Abstract

This overview paper includes both published and original data of the current state of the field of ^{51}V NMR in solid-state chemistry. Advantages and shortcomings of different NMR techniques in their applications to vanadium are discussed on the examples of their application to various vanadia based systems (including individual highly crystalline compounds, solid solutions, glasses, catalysts). New correlations between local structure of vanadium atoms and NMR parameters allowing to discriminate at least seven different types of vanadium sites (tetrahedral sites of Q^0, Q^1 and Q^2 types; trigonal pyramids of $3 = 1$ and $3 = 2$ (V_2O_5 like) types; tetragonal pyramids of $4 = 1$, $4 = 2$ types) are proposed. It is demonstrated that competent combination of different NMR approaches permits now not only to describe different vanadium sites in highly crystalline and amorphous materials, but also to insight into the structural aspects of disorder in crystallinity as well as to reveal the behavior of different functional groups at elevated temperatures. The influence of low valence vanadium atoms on ^{51}V NMR spectra is also discussed.

Keywords: Vanadium; Solid-state nuclear magnetic resonance; ^{51}V NMR; Ultra-high-speed MAS; MQMAS; SATRAS; STMAS; Individual compounds; Solid solutions; Glasses; Catalysts

1. Introduction

Among group V elements, vanadium is one of the most important element, widely used in solid-state chemistry, materials science, catalysis and engineering. Nowadays ^{51}V solid-state nuclear magnetic resonance (NMR) spectroscopy became a keystone technique for characterization of local structure of vanadium sites in different vanadium systems [1,2]. Modern NMR techniques such as ultra-high-speed MAS (35 kHz and higher), MQMAS, SATRAS allow to obtain direct and precise information on the local structure of vanadium sites: (i) the number of nonequivalent vanadium sites, (ii) coordination numbers, (iii) the nature of the atoms in the first coordination sphere, (iv) the distortion of this coordination sphere, (v) association of vanadium–oxygen polyhedron. In addition, spin echo mapping spectra or ultra-high-speed MAS experiments can highlight V^{5+} atoms bounded via oxygen atom by V^{3+} or V^{4+}; defects and distortions of the structure can be revealed by analysis of distributions of chemical shielding and quadrupolar tensor parameters. The main purpose of this work is to demonstrate current possibilities of ^{51}V NMR in solid-state chemistry, that is why there is

* Corresponding author.
E-mail address: olga@catalysis.nsk.su (O.B. Lapina).

0920-5861/02/$ – see front matter © 2002 Published by Elsevier Science B.V.
PII: S0920-5861(02)00299-7

no deep historical excursus in this field, as well as no complete bibliography. At present the bibliography in solid-state ^{51}V NMR applications counted hundreds papers, the review of them is for the future. In this paper, we considering only some results obtained by SATRAS, high-speed MAS (35 kHz), MQMAS, and STMAS, which demonstrate applicability of these techniques to various vanadia systems.

2. Modern solid-state ^{51}V NMR technique. Polycrystalline V^{5+} oxide compounds

^{51}V nucleus (natural abundance 99.76%) has a spin quantum number of $\frac{7}{2}$ and an electric quadrupole moment of 0.05 b, the relative intensity of ^{51}V NMR signal is 0.38 compared to an equal number of protons. In presence of a magnetic field, each vanadium nucleus of solid diamagnetic samples experiences, in general, three different types of interaction: (i) dipole interaction of its magnetic moment with magnetic moments of other nuclei, (ii) quadrupole interaction of its electric quadrupole moment with the electric field gradient, (iii) chemical shielding anisotropy (CSA) interaction. These interactions individually broaden and even shift (in the case of the quadrupolar interaction at second order) the observed lines, to such an extent that in static powdered solids, NMR has for long been accepted as of moderate value, until magic angle spinning (MAS) technique was introduced. Indeed, the extensive applicability of NMR to solids relies heavily on MAS. This technique is able to narrow the lines by successful averaging dipolar, anisotropic chemical shielding and first order quadrupolar effects. However, a residual line broadening issued from the quadrupolar interaction at second order remains and it has been until 1995 the main limitation of MAS resolution. Nevertheless, in the particular case of vanadium, the small value of electric quadrupole moment moderates the quadrupolar interaction and simple MAS technique, has proven to be a very convenient technique for vanadium characterization. The SAtellite TRAnsition Spectroscopy (SATRAS) [3,4] method has rapidly taken advantage of the MAS high-resolution spectra available for vanadium-containing sample. This technique allows a simple determination of the isotropic chemical shift (δ_{iso}) and composite quadrupolar coupling constant ($\lambda = C_Q\sqrt{1+\eta^2/3}$, $C_Q = e^2qQ/h$). In combination with automatic analysis (refinement) of the intensities of well-resolved satellite spinning sidebands the complete set of quadrupolar and CSA tensor parameters as well as their relative orientations can be measured. Thanks to SATRAS and spectral simulation, precise NMR data have been obtained for most of the individual vanadium-oxide compounds of the system V_2O_5–M_xO_y (M = mono-, di-, tri- and tetra-valent metals) [3–10].

Seven types of vanadium sites could be recognized based on the values of chemical shielding and quadrupolar tensors parameters obtained by SATRAS method for the above mentioned highly crystalline individual compounds with well known structures [3–10].

Tetrahedral vanadium sites of Q^0, Q^1 and Q^2 types could be revealed using correlation between the type (η_σ—chemical shielding asymmetry parameter) and value ($\Delta\sigma$—CSA) of chemical shielding anisotropy [1,2,11] (Fig. 1):

(i) Vanadium in regular tetrahedral oxygen environment (Q^0 type) has almost spherically symmetric chemical shielding tensor with small value of anisotropy ($\Delta\sigma < 100$ ppm); quadrupolar constant C_Q varies from 1 to 6 MHz; chemical shielding asymmetry parameter varies from 0 up to 1 [3,4,10].
(ii) Vanadium in slightly distorted tetrahedral sites with the adjacent tetrahedra sharing one common oxygen atom (Q^1 type) has an asymmetric chemical shielding tensor, but with larger value of anisotropy ($100 < \Delta\sigma < 200$ ppm); quadrupolar constant varies from 2.5 to 10 MHz; chemical shielding asymmetry parameter changes from 0.1 to 0.9 [3,4,10].
(iii) Vanadium in strongly distorted tetrahedral sites with adjacent tetrahedra sharing two common oxygen atoms (Q^2 type) has an asymmetric chemical shielding tensor with large value of anisotropy ($200 < \Delta\sigma < 500$ ppm); quadrupolar constant varies from 2 to 7 MHz; chemical shielding asymmetry parameters changes from 0.6 to 0.8 [3,4,10].

Whereas it is clear that vanadium sites in different pyramid couldn't be determined from Fig. 1. These sites could be recognized using

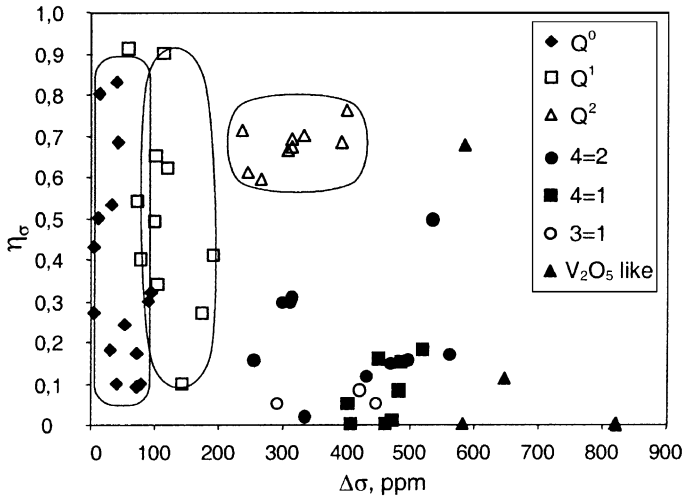

Fig. 1. Correlation between ^{51}V asymmetry (η_σ) and anisotropy parameters ($\Delta\sigma$) of chemical shielding tensor obtained for various vanadia compounds.

the correlation between *effective* $\sigma_\perp$ estimated as ($\sigma_\perp \sim 1/2(\sigma_1 + \sigma_2)$, σ_i—components of CS-tensor) and quadrupolar coupling constant (C_Q) for the case of a large value of CSA (200 ppm $< \Delta\sigma$) and $\eta_\sigma < 0.6$ (Fig. 2):

(iv) Vanadium in tetragonal pyramid of 4 = 2 type has an axially symmetric chemical shielding tensor with large value of anisotropy (200 $< \Delta\sigma <$ 500 ppm); quadrupolar constant varies from 4 to 8 MHz; chemical shielding asymmetry parameters changes from 0 to 0.6, $\sigma_\perp \sim$ 200–400 ppm [5–10].

(v) Vanadium in tetragonal pyramid of 4 = 1 type has an axially symmetric chemical shielding tensor with a large value of anisotropy (400 $< \Delta\sigma <$ 550 ppm); quadrupolar constant varies

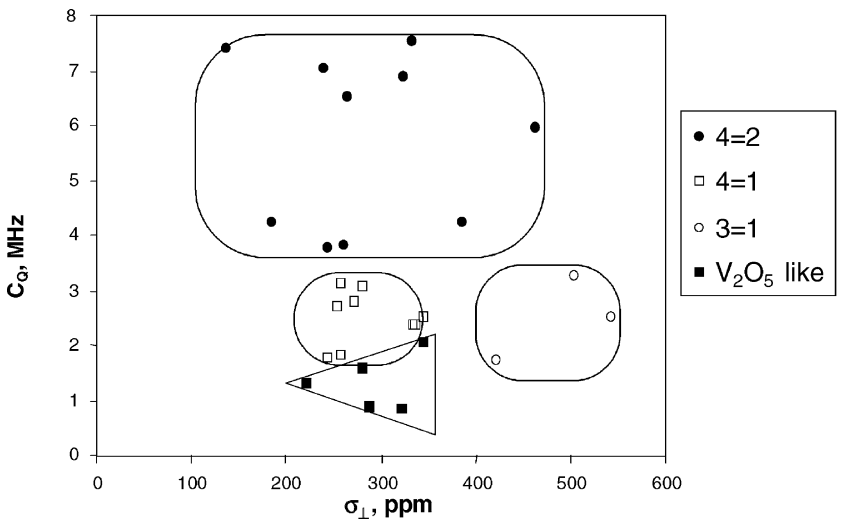

Fig. 2. Correlation between ^{51}V NMR chemical shielding tensor component ($\sigma_\perp$) and quadrupolar coupling constant (C_Q) for vanadium polyhedra with V=O bond having (200 ppm $< \Delta\sigma$) and $\eta_\sigma < 0.6$.

from 1 to 3 MHz; chemical shielding asymmetry parameters changes from 0 to 0.2, $\sigma_\perp \sim 200-400$ ppm [5–10].

(vi) Vanadium in trigonal pyramid of 3 = 1 type has an axially symmetric chemical shielding tensor with large value of anisotropy ($200 < \Delta\sigma < 500$ ppm); quadrupolar constant varies from 1 to 4 MHz; chemical shielding asymmetry parameters changes from 0 to 0.6, $\sigma_\perp \sim$ 400–600 ppm [5–10,12].

(vii) Vanadium in V_2O_5 like species (distorted octahedral or trigonal bipyramidal of 3 = 2 type) has an axially symmetric chemical shielding tensor with large value of anisotropy (500 ppm $< \Delta\sigma$); quadrupolar constant varies from 0 to 3 MHz; chemical shielding asymmetry parameters changes from 0 to 0.1, $\sigma_\perp \sim$ 200–350 ppm [5–10].

Thus based on the correlations presented in Figs. 1 and 2 seven different types of vanadia sites could be determined in vanadia systems (Fig. 3).

However, SATRAS has its own limitations, which are inherent to the resolution of the MAS technique. Spectra composed of nonequivalent vanadium sites with overlapping spinning sidebands may be difficult to analyze. In addition, defects and distortions of the structures broaden both, static and MAS spectra and further complicate the analysis. In these cases alternative techniques can be highly recommended. Spin-averaging approaches in combination with MAS have recently opened a new dimension in the spectroscopy of quadrupolar nuclei. In particular, the two-dimensional multiple quantum MAS (MQMAS) technique [13,14] correlates multiple quantum coherences with the single quantum coherence of the same spin (the central transition), thus achieving a high-resolution spectrum free of second-order broadening effects in one dimension. From the two-dimensional data matrix, the composite quadrupolar coupling constant and the isotropic chemical shift can easily be extracted. The simplicity of this technique has made it notably popular and applications have been reported on a variety of nuclei including sodium, rubidium, aluminum, oxygen, boron, niobium, cobalt, and numerous species with different spin quantum numbers that are characterized by a variety of coupling environments. However, it is commonly admitted that small value of quadrupolar moment and large value of CSA are a limitation to MQMAS and, in particular, prevent its application to vanadium nucleus [15].

Recently, we have demonstrated that a combination of ultra-high rotation frequency (30–35 kHz) with low power radio-frequency excitation allows the application of MQMAS to vanadium nucleus at all vanadium coordination [16]. For complex spectra with overlapping lines, MQMAS has significant privilege

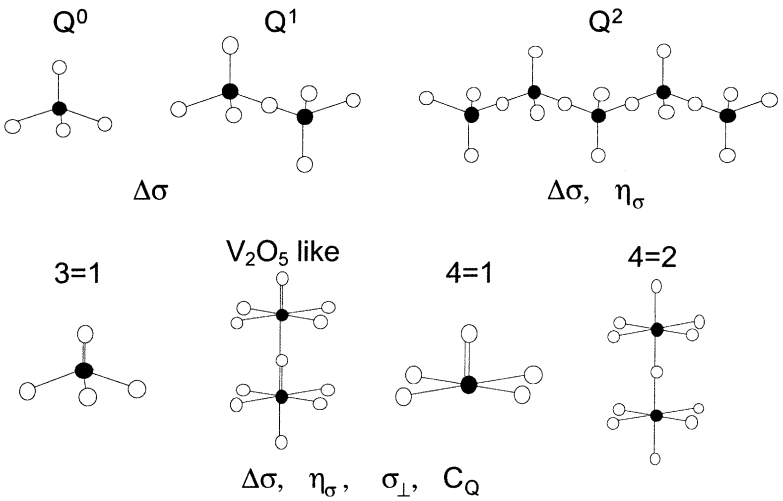

Fig. 3. The structures of vanadium sites, which could be determined from ^{51}V NMR parameters.

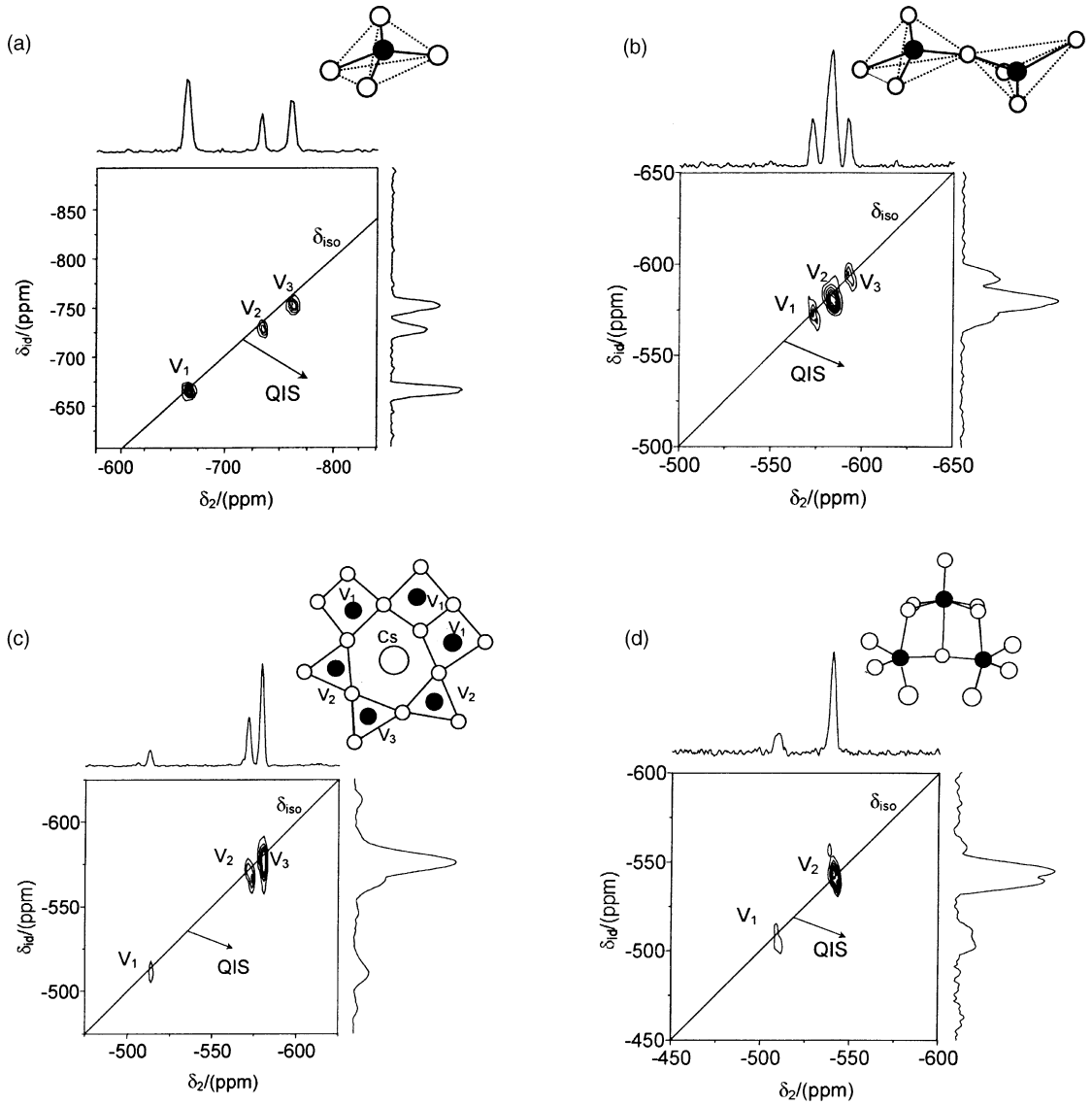

Fig. 4. ^{51}V 3QMAS spectra of $AlVO_4$ (a), $Ba_2V_2O_7$ (b), $Cs_2V_4O_{11}$ (c), $Rb_2V_6O_{16}$ (d). The experiments were recorded at a magnetic field of 9.4 T. A 2.5 mm MAS probe was used at spinning frequencies in the range 30–35 kHz. The three-pulse Z-filter sequence was employed for the recording of pure absorption 3QMAS spectra and 288 transients were recorded with 64 increments in the indirect dimension [16].

over SATRAS. Fig. 4 illustrates ^{51}V 3QMAS spectra of $AlVO_4$, $Ba_2V_2O_7$, $Cs_2V_4O_{11}$ and $Rb_2V_6O_{16}$, the crystalline structures of these compounds reveal from two to three nonequivalent vanadium sites. The resulting overlapping spinning sidebands observed in MAS, limit and sometime preclude SATRAS application for all these compounds, while the high resolution obtained in the 3QMAS spectrum allow a precise quantification of the isotropic chemical shift and λ parameter.

Fig. 4a shows the ^{51}V 3QMAS spectrum of $AlVO_4$. The crystalline structure is composed of three nonequivalent vanadium sites of type Q^0. High-resolution 3QMAS spectrum allows a precise quantifi-

Table 1
Composite quadrupolar coupling constant (λ) and isotropic chemical shift (δ_{iso}) measured by 3QMAS and SATRAS techniques[a]

	λ (MHz)		δ_{iso} (ppm)	
	3QMAS	1D	3QMAS	1D
$AlVO_4$	4.9 (0.7)	2.48[b]	−659.2 (1.4)	−662
	3.5 (0.9)	2.48[b]	−741.4 (1.4)	−743
	3.8 (0.8)	2.48[b]	−773.2 (1.4)	−776
$LaVO_4$	6.0 (0.5)	5.6	−604.8 (1.4)	−609
NH_4VO_3	3.1 (1.0)	2.95	−564.7 (1.4)	−563.7
$Rb_2V_6O_{16}$	2.47 (1.3)	3.12	−514.3 (1.4)	−515
	<1.8 (1.8)	2.37	−547.6 (1.4)	−547
$Cs_2V_4O_{11}$	1.9 (1.7)	1.29	−511.9 (1.4)	−513
	2.6 (1.3)	no[c]	−569.8 (1.4)	no
	2.4 (1.4)	1.81	−577.7 (1.4)	−575
$Ba_2V_2O_7$	2.27 (1.4)	2.25[b]	−579.6 (1.4)	−579
	3.5 (0.9)	2.25[b]	−587.8 (1.4)	−589
	1.1 (2.9)	2.25[b]	−599.6 (1.4)	−600

[a] For the 3QMAS experiments, errors are reported in brackets.
[b] The λ value could not be accurately determined by SATRAS and was estimated.
[c] Not observed.

cation of the isotropic chemical shift and λ parameter for each three sites. Fig. 4b shows the ^{51}V 3QMAS spectrum of $Ba_2V_2O_7$. In this sample, vanadium atoms are distributed between three nonequivalent Q^1 sites. As in the previous case a fully resolved 3QMAS spectrum was obtained (extracted NMR parameters with those obtained from SATRAS are given in Table 1). Fig. 4c and d shows the 3QMAS spectra of two compounds ($Cs_2V_4O_{11}$ and $Rb_2V_6O_{16}$) containing nonequivalent vanadium atoms with five or six coordination. In $Cs_2V_4O_{11}$ there are three types of vanadium sites: two in distorted tetrahedral pyramids and the third one with octahedral coordination. In $Rb_2V_6O_{16}$ there are two types of vanadium sites, both in octahedral coordination. The well resolved 3QMAS spectra obtained for these compounds allow to determine the isotropic chemical shift and the composite quadrupolar coupling constant. Though in $Rb_2V_6O_{16}$ both sites are observed, the low composite quadrupolar coupling constant of the weak line is not easily measured from the spectrum, only a maximum value of the quadrupolar coupling constant can be estimated.

These examples clearly illustrate the superiority of MQMAS over SATRAS, when several sites produce overlapping spinning sidebands. However, when the quadrupolar interaction is weak ($C_Q < 1$ MHz) the incertitude on its quantification may be large.

Recently, the satellite transition MAS (STMAS) [17,18] technique has been proposed as an alternative method to MQMAS. STMAS is expected to give better sensitivity and be less dependant on CSA and strength of the quadrupolar interaction (sites with low or high quadrupolar coupling constants should be more easily observable in STMAS than in MQMAS). The STMAS has significant similitude with both MQMAS and SATRAS experiments: it correlates in a two-dimensional spectrum the central transition with the satellite transitions (m, $m-1$), and in fact STMAS experiment can be described as a two-dimensional SATRAS experiment. STMAS experiment requires a very accurate setting of the magic angle (as for SATRAS). Quantitatively, it has been shown, on a ^{23}Na STMAS experiment on Na_2SO_4, that an angle offset of 0.016° has significant line broadening effects [18]. On conventional probes, such an accurate angle setting is not without inherent technical difficulties. Eq. (1) gives the full linewidth $\Delta\nu_{Fl}$ along the isotropic dimension (after shearing) of the STMAS spectrum [18]:

$$\Delta\nu_{Fl} \cong \frac{3\sqrt{2}C_Q}{I(2I+1)}\Delta\theta \quad (1)$$

C_Q is the quadrupolar coupling constant ($C_Q = e^2qQ/h$) and $\Delta\theta$ (rad) the angle offset from the magic angle. Eq. (1) shows that the linewidth $\Delta\nu_{Fl}$ is directly proportional to the product of the quadrupolar coupling constant by the angle offset. This clearly indicates that, the stronger is quadrupolar coupling, the more precisely magic angle has to be set. In addition, the spin quantum number being involved at the denominator of Eq. (1), the adjustment of the magic angle should be less demanding as this number increases. These two points are indeed, favorable to vanadium nuclei. The high spin quantum number of $\frac{7}{2}$ and the generally weak quadrupolar coupling constants observed for vanadium atoms should permit small departures from the exact magic angle position. In principle, SATRAS spectra are composed of as many lines as the number of (m, $m-1$) transitions, and it is, for the moment, not possible to select one particular satellite transition other than by adjusting radio-frequency fields power in order to emphasize the desired transition. The autocorrelation signal of the central

transition can be removed by selective presaturation or by subtraction of a spectrum of the solely autocorrelation signal [19] but these may be of poor efficiency for removing unwanted satellite transitions. In the case of spin $\frac{7}{2}$ the STMAS spectrum is composed in principle, of the correlation of central transition $(-\frac{1}{2}, \frac{1}{2})$ with itself plus three satellite transitions $(\frac{1}{2}-\frac{3}{2}, \frac{3}{2}-\frac{5}{2}, \frac{5}{2}-\frac{7}{2})$. This multiplicity of signal may complicate the interpretation of spectra when several sites are involved.

Up to now STMAS has been applied to ^{27}Al and ^{23}Na, and ^{17}O [20] in ^{17}O enriched Mg_2SiO_4. Herein we report the first ^{51}V STMAS experiment. Fig. 5 shows the ^{51}V STMAS spectrum of $LaVO_4$, three signals are observable: (i) the central transition signal (CT), (ii) the $(\frac{1}{2}-\frac{3}{2})$ satellite signal (ST1), (iii) the $(\frac{3}{2}-\frac{5}{2})$ satellite signal (ST2). The composite quadrupolar coupling constant and the isotropic chemical shift extracted from the position of the center of gravity of the ST1 line ($\lambda = 6.2$ MHz, $\delta_{iso} = -605$ ppm) and those resulting of the frequencies of the center of gravity of ST2 ($\lambda = 6.0$ MHz, $\delta_{iso} = -600$ ppm) agree with SATRAS and MQMAS data [21]. The intensity of the correlation line with the $(\frac{5}{2}-\frac{7}{2})$ transition (ST3 signal) in not visible in Fig. 5 because its intensity is too low (about the noise level) and below the floor used to draw the contour plots.

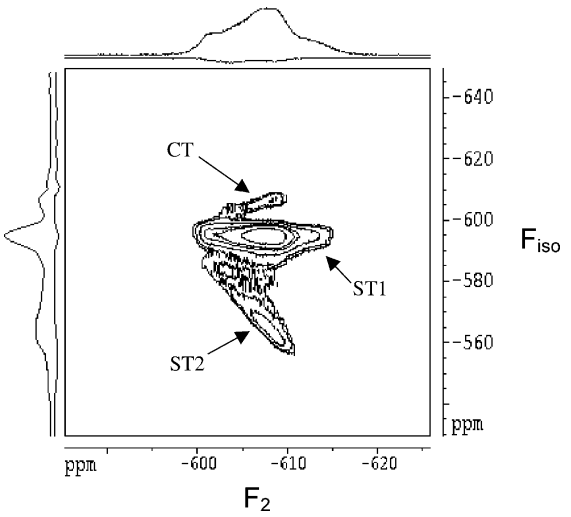

Fig. 5. ^{51}V STMAS spectrum of $LaVO_4$ obtained after shearing (the shearing has been chosen to produce an isotropic line for the ST1 signal in the indirect dimension), showing the different correlations: (CT) is the autocorrelation of the central transition, ST1 correlates the central transition with the $(\frac{1}{2}-\frac{3}{2})$ satellite transition and ST2 correlates the central transition with the $(\frac{3}{2}-\frac{5}{2})$ satellite transition. The experiment has been recorded in a magnetic field of 9.4 T, at a spinning frequency of 10 kHz, 256 transients have been accumulated. On both axes positive and negative skyline projections are shown.

3. Vanadium in lower oxidation states

Whilst V^{5+}-containing phases can be easily characterized by conventional ^{51}V MAS NMR, this is not the case for materials with vanadium atoms in lower oxidation states. However, information concerning the nature, location and oxidation state of vanadium centers can indirectly be obtained from NMR spectra of neighboring atoms. Thus, on vanadium–phosphorus system, Gerstein and coworkers [22] and later Tuel et al. [23] has applied a ^{31}P spin echo mapping technique, which allows to evidence vanadium paramagnetic centers by observing a large ^{31}P spectral region. For V^{5+} containing compounds ^{31}P chemical shift is in the range 20–40 ppm; for compounds containing V^{4+} phosphorous chemical shift varies from 1600 to 2600 ppm; for V^{3+} containing compounds ^{31}P chemical shift is near 4650 ppm. These shifts are of the Fermi-contact origin, and can be used as a measure of the unpared electron spin density transferred from the paramagnetic centers to the ^{31}P nucleus. Thus, ^{31}P line shift gives direct indication on the number of paramagnetic species in the first coordination sphere of phosphorus as well as on their oxidation state.

We have decided to extend the ^{31}P spin echo mapping technique to $^{51}V^{5+}$, in ultra-high-speed MAS (and large spectral width) conditions, in order to detect by observing ^{51}V NMR signal of V^{5+} atoms, the proximity of vanadium atoms in a lower oxidation state. Bronzes and oxovanadium sulfate have been used as an example of mixed V^{5+} and V^{4+} valence compounds. NaV_6O_{15} formally contains five V^{5+} ions per one V^{4+} ion. According to the structural data each vanadium ion has two nearest vanadium neighbors at 3.06 Å. In this compound ^{51}V isotropic chemical shift is observed at -900 ppm. For $Bi_6V_3O_{16}$ (there is one V^{4+} ion per two V^{5+} ions) isotropic shift is equal to -1447 ppm [24]. $K_6(VO)_4(SO_4)_8$ contains V^{4+}/V^{5+} pairs of VO_6 distorted octahedral

units, usually possessing one short V=O bond about 1.57 Å, and four equatorial bonds around 2.00 Å [25]. Eight different SO_4^{2-} groups form bidentate bridges between the V^{4+} and V^{5+} ions. It is worth noting that the CSA (635 ppm) and the isotropic shift (−655 ppm) of this compound are close to those observed for pure V^{5+} oxosulfatovanadates (compounds formed in V_2O_5–$M_2S_2O_7$ system). The latter indicates that the distance (SO_4 bridge) between V^{4+} and V^{5+} along with the short electron spin relaxation time for V^{4+} is sufficient to reduce significantly the influence of paramagnetic V^{4+} on diamagnetic V^{5+}. Thus, ^{51}V NMR line shift gives implicit indication on the number of V^{4+} ions in the first coordination sphere as well as on the distance between V^{5+} and V^{4+}.

Different positions concerning the influence of V^{3+} on ^{51}V NMR spectra of V^{5+} ions exist in the literature. Boyarski et al. [26] claims to have directly observed V^{3+} and V^{5+} NMR signals in V_2O_4 (which is proposed to contain vanadium atoms in both states). On the other hand, Pons et al. [27] states that the presence of V^{3+} prevents observation of ^{51}V resonance. We have checked the ^{51}V NMR spectrum of V_2O_4, at 35 kHz a signal significantly shifted to a lower field up to 2100 ppm has been observed. The same spectrum was observed recently by Jakobsen and coworkers [28] and has been assigned to V^{4+} coupled to the neighbouring V^{4+} with the formation of diamagnetic site.

4. Solid solutions, glasses, melts (structure, dynamics)

Solid-state NMR methodology progresses take advantage of the possibility to probe highly crystalline and/or amorphous phases to give new insights into the structural aspects of disorder in crystalline and glassy solid solutions. In these systems, ion mobility can be characterized over a large timescale by several NMR approaches. Atomic and molecular mobility occurring with correlation times of the order of a millisecond can be monitored from variable-temperature static solid-state NMR. Furthermore, temperature and frequency dependency measurements of nuclear spin–lattice relaxation rates afford a comprehensive characterization of internal dynamics of solids occurring on a microsecond timescale.

4.1. Solid solutions $MNb_{2(1-x)}Ta_{2x}VO_9$

Substitutional solid solutions $MNb_{2(1-x)}Ta_{2x}VO_9$ with different M and x (for M = La, x = 0, 0.1, 0.16, 0.2, 0.25, 0.3; for M = Y, x = 0, 0.1, 0.2, 0.29, 0.38, 0.58; for M = Sc, x = 0, 0.3, 0.5, 0.7, 1.0) have been characterized by ^{51}V SATRAS technique. Variation of M and x allows structural investigations of solid solutions to be made using the replacement of some atoms in the cation sublattice (M) and in the anion sublattice (x). The structure of vanadium anion sublattice is the same for M = La and Y, while for M = Sc, it becomes

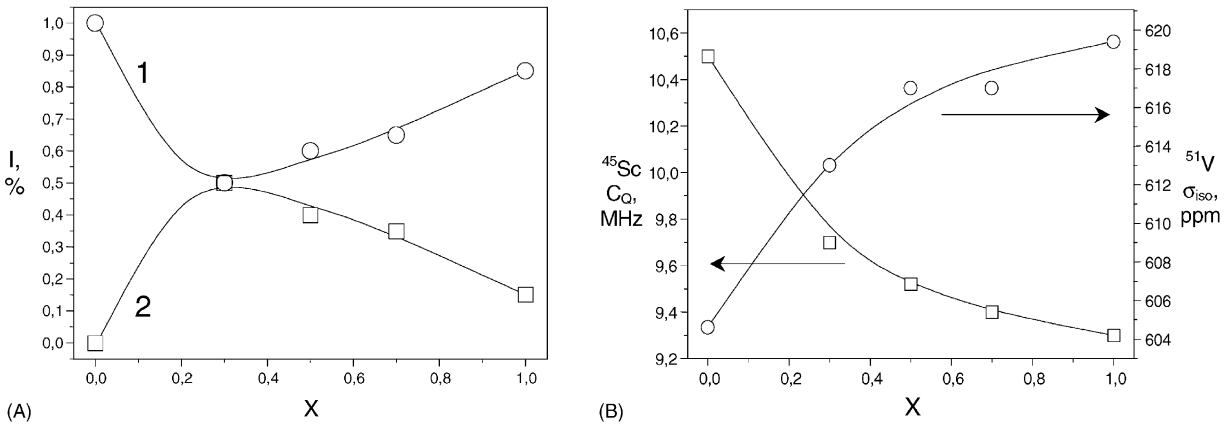

Fig. 6. (A) Relative intensities of ^{51}V NMR lines from tetrahedral (1) and octahedral (2) vanadium sites in the solid solution $ScNb_{2(1-x)}Ta_{2x}VO_9$ depending on x; (B) changes of σ_{iso} for tetrahedral vanadium sites and C_Q on ^{45}Sc depending on x.

rather complex. These three elements belong to the same 3B group and have identical valence (3+), but they differ by their ionic radii 0.81 Å (Sc^{3+}), 0.97 Å (Y^{3+}), 1.06 Å (La^{3+}). Ionic radius of Sc^{3+} is 23.6% smaller than the La^{3+} one, while Y^{3+} ionic radius is only 8.5% smaller. This can explain the different anion structure sublattice formation for Sc solid solutions. For M = La and Y, vanadium sublattice is composed of isolated regular tetrahedra of Q^0 type. While for M = Sc, vanadium anion sublattice is represented by the superposition of distorted octahedral and regular tetrahedral sites. Variation of x (replacement in anion sublattice) results in monotonic changes in the values of chemical shifts and linewidths both for ^{51}V and ^{45}Sc (Fig. 6). Replacement of Nb by Ta is accompanied by monotonic changes of relative concentration of octahedral and tetrahedral sites in Sc system (Fig. 6) [29].

4.2. $M_2S_2O_7$–V_2O_5 and $MHSO_4$–V_2O_5 (M = Na, K, Cs) glasses, melts: structure and dynamic behavior of the framework units

Valuable information about glass and melt structures as well as about dynamical behavior of framework units may be obtained from temperature-dependent studies of melt-quenched glasses, which are accepted to retain the main structural features of the melt. Exchange processes observed at T_g are supposed to be the most important for melts. This approach has been chosen for the NMR study of $M_2S_2O_7$–V_2O_5 (M = Na, K, Cs) melts [30–32].

At ambient temperature the static ^{51}V NMR spectra of melt-quenched $M_2S_2O_7$–V_2O_5 glassy samples are similar for a wide range of composition. They show a broad line with an axial anisotropy of the chemical shielding tensor corresponding to vanadium atoms in a distorted octahedral oxygen environment with one short V=O bond. They exhibit a Gaussian-like distribution of the quadrupole coupling constant which is typical for glassy samples. As the vanadium concentration increases, chemical shielding tensor parameters distribution also increases indicating a more disordered local environment of vanadium sites.

^{23}Na, ^{39}K and ^{133}Cs NMR experiments confirm the lack of long-range order in the glassy samples. According to these data cations are randomly distributed over the vanadium sulfate framework. At room temperature there is no chemical exchange of cations between different sites. This exchange is only observed at elevated temperatures, when simultaneously, a remarkable transformation of the anion framework takes place.

Two different ways of crystallization were revealed during heating of the melt-quenched glassy samples. The type of crystallization, in the studied glasses, depends on the local and extended arrangement of structural units. If the glass structure is similar to the crystal structure of the compounds formed at a given composition, the glass–crystalline transition (at T_g) is similar to a solid–solid transition. Then, crystallization requires only moderate changes of the anion framework and cations sublattice. However, if the composition of the crystalline compounds differs significantly from the starting glass composition, the glass framework needs essential rearrangement. Then, a glass-to-crystal transition follows through the so-called “metastable liquid state”. All these processes may be easily traced by NMR.

As an example, the ^{51}V NMR static spectra, recorded for heated $4Cs_2S_2O_7$–V_2O_5 and $2Cs_2S_2O_7$–V_2O_5 melt-quenched glasses are shown in Fig. 7. At ambient temperature both spectra exhibit broadened lines with axial CSA. When the $4Cs_2S_2O_7$–V_2O_5 sample is heated to 200–220 °C the spectrum transforms to a narrow symmetric line. This isotropic averaging of CSA indicates a high mobility of vanadium-containing species, usually occurring in liquids. A visual observation of the metastable liquid at this temperature (T_g for this sample) supports this conclusion. Simultaneously, cations mobility sharply increases, as follows from the ^{133}Cs NMR spectrum measured at the same temperature. As the sample is kept at T_g, the metastable liquid crystallizes into crystalline $Cs_2S_2O_7$ and $Cs_4(VO)_2O(SO_4)_4$. Since the Cs/V molar ratio of the crystalline compound (Cs/V = 2) differs from that of the starting glass composition (Cs/V = 4), crystallization indeed proceeds through the metastable liquid state. On the contrary, in the case of $2Cs_2S_2O_7$–V_2O_5 glass composition, the ratio Cs/V (2) is equivalent to that of $Cs_4(VO)_2O(SO_4)_4$, and the glass-to-crystal transition is fast without detection of a metastable liquid. As crystallization completes, the anion framework stabilizes and is maintained during subsequent heating, up to the melting point. At the same time in both cases, the cation mobility continuously increases with the increasing temperature.

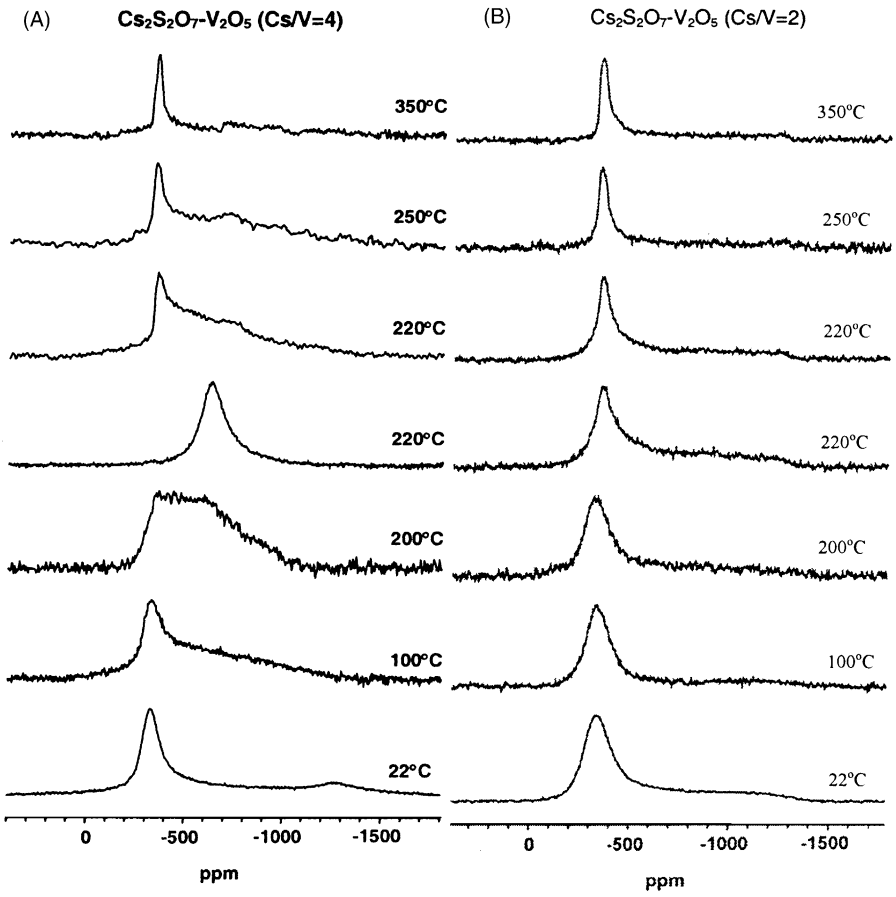

Fig. 7. ^{51}V NMR spectra of melt-quenched glassy samples: (A) $Cs_2S_2O_7$–V_2O_5 (Cs/V = 4); (B) $Cs_2S_2O_7$–V_2O_5 (Cs/V = 2) measured at indicated temperatures. NMR spectra have been measured on a Bruker MSL-400 spectrometer (magnetic field 9.4 T) using homemade high temperature NMR probe [30].

Fig. 8 shows the ^{51}V spectra of $(1-x)K_2S_2O_7$–xV_2O_5 melts. A narrow line is observed at −587 ppm for the pure V_2O_5 melt. The increase of the chemical shift from −612 ppm (solid) to −587 ppm (liquid), indicates the changes of vanadium coordination from octahedral (solid) to tetrahedral (melt). This decrease in the coordination number under melting is typical for transition metal oxides. ^{51}V NMR relaxation times may help to estimate the average size of the oxovanadium species in the V_2O_5 melt. These species are found to exist as short one-dimensional chains of several tetrahedral VO_4 units. The chains are small in size, and quadrupole broadening is most likely removed by their fast rotation.

Small amounts of pyrosulfate or hydrogensulfate added to vanadium pentoxide melts essentially broaden the ^{51}V NMR line (thus at $x = 0.98$, linewidth is broadened by about a factor of 4). Conceivably individual vanadia $(VO_4)_n$ chains are laced with oxosulfate links coordinated to vanadium. In this case the mobility of $(VO_4)_n$ chains should sharply decrease, resulting in a quadrupole broadening of ^{51}V NMR line. Such broadening in melts with $x = 0.1$–0.3 completely excludes the observation of any NMR line, since large bulk three-dimensionally interacting species are formed.

Similar behavior is observed in the melts with low vanadium content. In the pyrosulfate system, vana-

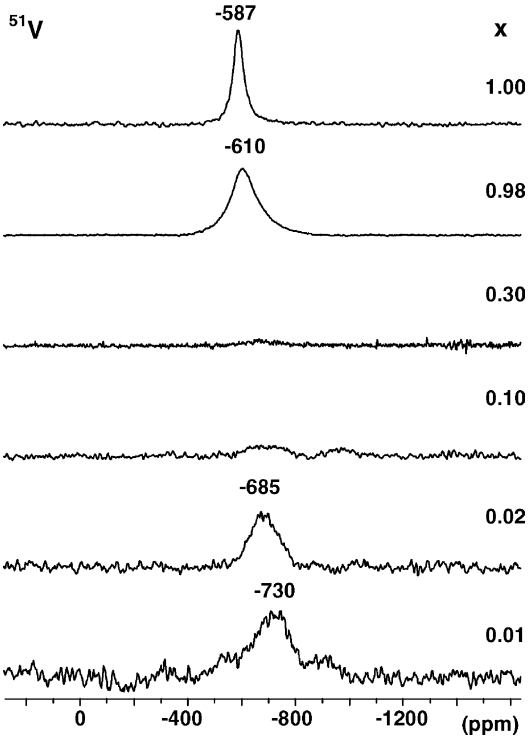

Fig. 8. ^{51}V NMR spectra of the $K_2S_2O_7$–V_2O_5 melts with varied vanadium concentrations. NMR spectra have been measured on a Bruker MSL-400 spectrometer (magnetic field 9.4 T) using homebuild high temperature NMR probe [32].

dium may exist (at low concentrations) in the form of monomeric vanadium-oxosulfate complexes (this is corroborated by some ^{17}O NMR measurements). The fast rotational mobility of such complexes diminishes the broadening mechanism (quadrupolar broadening) and, ^{51}V signals can then be observed. The line position (chemical shift at about −730 ppm) indicates an octahedral oxygen coordination of vanadium atoms (it is tetrahedral in pure V_2O_5 melt). The increase in vanadium content results in the dimerization and oligomerization of the vanadium-oxosulfate units. A large size of the oligomeric species prevents observation of their ^{51}V NMR spectra due to mobility decrease and effective quadrupolar broadening.

Thus, NMR data show that the type of vanadium species in the melts depends on vanadium concentration. At low vanadium concentration, the formation of monomeric or not associated dimeric complexes is likely in the pyrosulfate system. The increase of the vanadium concentration above 0.1 leads to association of the complexes with the formation of dimeric $(VO)_2O(SO_4)_4^{4-}$ and finally oligomeric species at $x > 0.3$. Further increase of the vanadium content diminishes the number of sulfate or pyrosulfate anions coordinated to vanadium. In the melt of the pure V_2O_5 the chains of VO_4 tetrahedra bridged via common oxygen atoms are retained. As was expected, alkali cations are characterized by high diffusion mobility in the melts.

5. Solid catalysts

Last decade, numerous papers devoted to ^{51}V NMR studies of solid vanadia based catalysts have been published, demonstrating NMR importance and self-descriptiveness for so complex systems as catalysts. It is worth noting that valuable data concerning structure of different binary catalysts, catalysts modified by different promoters, as well as binary catalysts prepared on mixed oxide supports have been obtained (these results were reviewed partly in the encyclopedia of nuclear magnetic resonance spectroscopy [2]). Nevertheless, the last few years ‘revolution’ in the solid-state NMR spectroscopy of quadrupolar nuclei with half integer spin has revealed new approaches and possibilities for ^{51}V NMR, especially in its application for characterization of different vanadia catalysts. Herein the possibilities of ultra-high-speed MAS (35 kHz) and MQMAS NMR will be shown on the example of supported VO_x/TiO_2 catalysts.

Different methods are used for preparation of model and real VO_x/TiO_2 catalysts, among them: deposition of thin V_2O_5 layers on clean anatase single crystal, grafting of $VOCl_3$ from gas phase or $VOCl_3$ (VOR_3) from inert solutions on polycrystalline TiO_2, impregnation of polycrystalline TiO_2 by different solutions containing V^{5+} or V^{4+} salts, equilibrium impregnation at different pH, ultra-high intensity grinding of the mixture of initial oxides V_2O_5 and TiO_2, and coprecipitation of mixed vanadia–titania solutions with special drying techniques (so-called spray-drying). These techniques result in different bonding between vanadium and titanium atoms. The gentler interaction is expecting to occur during the deposition of thin V_2O_5 layers on anatase single crystal. Only surface species should be formed during chemical reaction between

VOR_3 and surface hydroxyl groups (grafting). While its is impossible to exclude the formation of bulk vanadium sites during impregnation and milling procedures, bulk vanadium sites should be mainly formed under coprecipitation techniques. In order to reveal the structure of active sites it is necessary to know the structure of surface vanadium species and bulk vanadium sites, as well as the concentration of the surface vanadium species and their catalytic activity.

Grafting technique is achieved through chemical reaction between hydroxyl groups of the support surface with supported vanadium compound ($VOCl_3$): $VOCl_3 + n(HO–Ti–) \rightarrow VOCl_{3-n}(O–Ti–)_n$, where n can be 0–3. According to ^1H NMR data only the bridging OH groups react with chlorine atoms of $VOCl_3$. Isotropic chemical shift and chemical shielding anisotropy measured by ^{51}V MAS NMR indicate that two chlorine atoms are simultaneously involved in this reaction. As a result vanadium is bounded with TiO_2 surface via two oxygen bonds with the formation of tetrahedral surface species, characterized by one short vanadium–oxygen bond and a V–Cl bond.

After hydration–dehydration procedures, three groups of signal (group I composed of the lines situated between −515 and −530 ppm, group II situated between −560 and −580 ppm and group III between −610 to −660 ppm) are formed (Fig. 9a) [33]. Note especially, that for the first time the spectra of samples were measured at spinning frequency of 35 kHz. That allowed definite separation of all the isotropic lines from the spinning sidebands. The high field shift of the lines of the group III is likely due to the strong interaction between vanadium and Ti (for example, via two or three bonds). It is possible to suggest that the lines of group I correspond to vanadium weakly bound to Ti (for example, via one or two bonds). Each group of signal consists of two or three lines that may result from the interaction of supported vanadium with OH groups located not only on the densest TiO_2 plane (0 0 1), but also on cleavage planes other than (0 0 1). Observation of 6–9 nonequivalent vanadium sites indicates that there should be also an association of vanadium species.

These lines have distinct behaviors under H_2O or NH_3 adsorption (confirming the formation of several different vanadium sites on TiO_2 surface). Low temperature (20 °C) ammonia adsorption (Fig. 9b) preferentially affects sites of group III. At higher

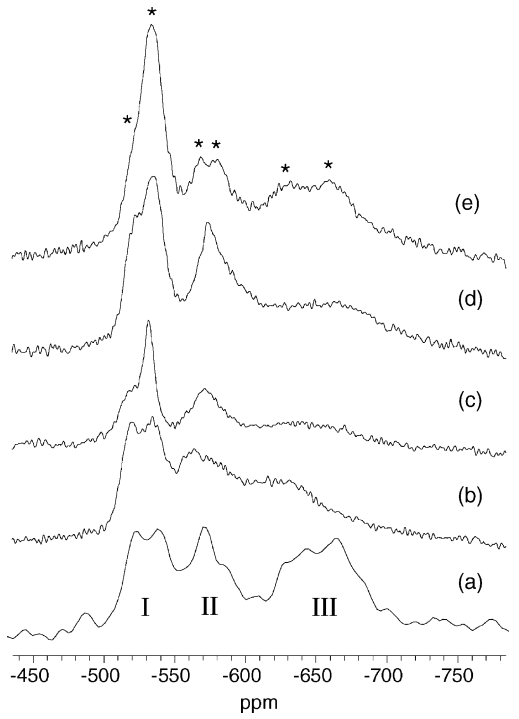

Fig. 9. ^{51}V MAS NMR spectra of VO_x/TiO_2 catalyst prepared by grafting method ($\nu_r = 35$ kHz), at this rotational frequency there is no overlapping between isotropic lines and spinning sidebands. only isotropic lines, marked by asterisks are shown: (a) spectrum of initial catalyst; (b) after NH_3 adsorption at 20 °C; (c) after NH_3 adsorption at 200 °C; (d) after NH_3 adsorption at 350 °C; (e) after running in catalytic reaction at 350 °C (a treatment in stronger conditions reverts spectrum (e) to the initial one).

temperatures (Fig. 9c and d) attenuation of the signals of group I is detected, and low field shifted peak is becoming less intense. Note that group II presents the steadiest response to exposure to NH_3. The formation of a great number of vanadium species on the catalyst surface was confirmed also by some DRIFT measurements.

The species structures significantly change after catalytic reaction: the main line corresponds to vanadium sites of group I. Integrated intensity of group III peaks decreases, while that of group II remains unchanged (Fig. 9e). Hydroxylation of group III sites and conversion of group I sites can thus be proposed. High mobility of the protons on the catalyst surface additionally facilitated by the coarse of reaction supports this statement.

Catalysts prepared by spray-drying method are characterized by a strong interaction between initial oxides with the formation of the coherent interfacial boundary between TiO_2 and V_2O_5. Vanadium atoms forming this boundary have an octahedral environment, which is less axial than in V_2O_5 [34]. Large value of quadrupolar constant indicates significant structural distortions (probably, in the second coordination sphere) of the local environment of V^{5+} localized in interfacial boundary in comparison with the local environment of V^{5+} ions in bulk V_2O_5.

The appearance of the common boundary between vanadia and titania particles has been noticed in the samples prepared with ball milling followed by the thermal treatment, but in this case there is the other stacking geometry. According to ^{51}V NMR two different types of octahedrally coordinated vanadium (V^{5+}) species (V^{5+} (I) and V^{5+} (II)) strongly bonded to TiO_2 are formed in milling samples [35]. During milling–calcination processes an increase of V^{5+}(I) and V^{5+}(II) concentrations is observed with the appearance of V^{3+} ions, along with the formation of at least three different types of paramagnetic V^{4+} species. Relative amounts of different V^{4+} and V^{5+} species depend on the milling time, presence of H_2O in the system, and subsequent calcination procedures (temperature and calcination time). Thus, V^{5+}(I) species are formed predominantly during milling, whereas those of V^{5+}(II) after the thermal treatment. For the structural characterization of these species, complete sets of the quadrupole and chemical shielding tensor parameters, including relative tensor orientation, have been estimated by SATRAS technique. This leads to the conclusion that the octahedral environment of vanadium in V^{5+} (II) species is less distorted than in V^{5+} (I), and in both cases the distortion is less axial than in V_2O_5.

Comparison of these data with catalytic activity of the samples and with theoretical calculations suggests the structure of active sites and also the mechanism of catalytic reaction [35].

Bright results were obtained by SATRAS and MQMAS techniques for doped vanadia catalysts [36,37]. Phosphorous-doped VO_x/TiO_2 catalysts prepared by the spray-drying method and treated under catalytic reaction have been studied by SATRAS, 2D triple-quantum, quintuple-quantum MAS NMR, and spin echo mapping methods. The simultaneous determination of CSA and quadrupole tensor parameters, as well as their distributions, permits to draw a conclusion on the local environment of vanadium sites in the catalysts. The formation of a triple V–P–Ti compound in phosphorous-doped VO_x/TiO_2 catalysts has been revealed. Only one type of slightly distorted tetrahedral vanadium atoms bound via oxygen to phosphorous was found in this compound. The very large distribution of the quadrupole coupling constant points to the irregular structure of this compound [36].

Sodium-doped binary vanadia–titania catalysts prepared by the spray-drying method and treated under catalytic reaction have been studied using fast MAS and two-dimensional triple-quantum MAS NMR [37]. Several vanadium-containing species have been identified in a representative set of catalysts of various sodium contents. Analysis of both ^{23}Na and ^{51}V NMR spectra has provided relative contents of sodium and vanadium compounds. Similar to potassium-modified catalysts, sodium vanadate is formed at high concentrations of alkali metal (sodium), while at low concentrations of Na a vanadium bronze of NaV_6O_{15} composition arises. The preferential formation of sodium vanadate is the cause of an effective decrease in content of strongly bound vanadium. At the same time, a part of the sodium readily interacts with residual sulfate ions, and a considerable amount of sodium sulfate was found with ^{23}Na 3QMAS NMR. The use of multiple-quantum sodium NMR has allowed the evaluation of the isotropic chemical shifts and λ parameters for all of the observed sodium species.

6. Conclusions

The results presented in the paper demonstrate advantages and limitations of modern solid state ^{51}V NMR techniques (SATRAS, high-speed MAS (35 kHz), MQMAS, STMAS). Some examples illustrate applications of these techniques to various vanadium systems, including individual crystalline compounds, solid solutions, glasses and catalysts. Original correlations of the structure of vanadium atoms and NMR parameters are proposed allowing discrimination of at least 7 different types of vanadium sites (tetrahedral sites of Q^0, Q^1 and Q^2 types; trigonal pyramids of $3 = 1$ and $3 = 2$ (V_2O_5-like) types; tetragonal pyramids of $4 = 1$ and $4 = 2$ types.

It is demonstrated that appropriate combination of different NMR techniques permits now not only to identify different vanadium sites in crystalline and amorphous materials, but also to get insight into the structural aspects of disorder and temperature behavior of different functional groups. The effect of vanadium atoms in low oxidation states on ^{51}V NMR spectra is also discussed.

Acknowledgements

This work was partly supported by RFBR grant 01-03-32364 and PAI 04522WK. C. Huguenard and C. Morais are thanked for their help with the STMAS experiment. L.G. Pinaeva, V.N. Bondareva, K.V. Romanenko, G.A. Zenkovets, H. Knözinger, M.G. Zuev are thanked for their help and important discussions.

References

[1] O.B. Lapina, V.M. Mastikhin, A.A. Shubin, V.N. Krasilnikov, K.I. Zamaraev, Prog. NMR Spectrosc. 24 (1992) 457.
[2] V.M. Mastikhin, O.B. Lapina, in: D.M. Grant, R.K. Harris (Eds.), Encyclopedia of NMR (Nuclear Magnetic Resonance), vol. 8, Wiley, Chichester, UK, 1996, p. 4892.
[3] C. Jäger, J. Magn. Reson. 99 (1992) 353.
[4] J. Skibsted, N.C. Nielsen, H. Bildsøe, H. Jakobsen, Chem. Phys. Lett. 188 (1992) 405.
[5] J. Skibsted, N.C. Nielsen, H. Bildsøe, H.J. Jakobsen, J. Am. Chem. Soc. 115 (1993) 7351.
[6] J. Skibsted, C.J.H. Jacobsen, H.J. Jakobsen, Inorg. Chem. 37 (1998) 3083.
[7] U.G. Nielsen, H.J. Jakobsen, J. Skibsted, Inorg. Chem. 39 (2000) 2135.
[8] U.G. Nielsen, H.J. Jakobsen, J. Skibsted, J. Phys. Chem. B 105 (2001) 420.
[9] C.J. Fontenot, J.W. Wiench, M. Pruski, G.L. Schrader, J. Phys. Chem. B 105 (2001) 10496.
[10] D.F. Khabibulin, A.A. Shubin, O.B. Lapina, NATO ASI, Magnetic Resonance in Colloid and Interface Science, (2002) 537–545.
[11] V.M. Mastikhin, O.B. Lapina, V.N. Krasilnikov, A.A. Ivakin, React. Kinet. Catal. Lett. 24 (1984) 119.
[12] N. Das, H. Eckert, H. Hu, I.E. Wachs, J.F. Walzer, F.J. Feher, J. Phys. Chem. 97 (1993) 8240.
[13] L. Frydman, J.S. Harwood, J. Am. Chem. Soc. 117 (1995) 5367.
[14] A. Medek, J.S. Harwood, L. Frydman, J. Am. Chem. Soc. 117 (1995) 12779.
[15] A. Medek, L. Frydman, J. Magn. Reson. 138 (2) (1999) 298.
[16] O.B. Lapina, P.R. Bodart, J.-P. Amoureux, NATO ASI, Magnetic Resonance in Colloid and Interface Science, (2002) 355–365.
[17] Z. Gan, J. Am. Chem. Soc. 122 (2000) 3242.
[18] Z. Gan, J. Chem. Phys. 114 (2001) 10845.
[19] C. Hugenard, F. Taulelle, B. Knott, Z. Gan, J. Magn. Reson. 156 (2002) 131.
[20] K.J. Pike, S.E. Ashbrook, S. Wimperis, Chem. Phys. Lett. 345 (2001) 400.
[21] P.R. Bodart, J. Magn. Reson., accepted for publication.
[22] J. Li, M.E. Lashier, G.L. Schrader, B.C. Gerstein, Appl. Catal. 73 (1991) 83.
[23] A. Tuel, L. Canesson, J.C. Volta, Coll. Surf. A 158 (1999) 97.
[24] F. Delmaire, M. Rigole, E.A. Zhilinskaya, A. Aboukais, R. Hubaut, G. Mairesse, Phys. Chem. Chem. Phys. 2 (19) (2000) 4477.
[25] K.M. Eriksen, K. Nielsen, R. Fehrmann, Inorg. Chem. 35 (1996) 480.
[26] L.A. Boyarski, S.P. Gabuda, S.G. Kozlova, Low Temp. Phys. 26 (2000) 147.
[27] A.L. Pons, X. Lin, J.J. Fripiat, Solid State Ionics 84 (1996) 213.
[28] U.G. Nielsen, J. Skibsted, H.J. Jakobsen, Chem. Phys. Lett. 356 (2002) 73.
[29] O.B. Lapina, D.F. Khabibulin, K. Romanenko, M.G. Zuev, in preparation.
[30] O.B. Lapina, V.V. Terskikh, A.A. Shubin, V.M. Mastikhin, K.M. Eriksen, R. Fehrmann, J. Phys. Chem. 101 (1997) 9188.
[31] O.B. Lapina, V.V. Terskikh, A.A. Shubin, K.M. Eriksen, R. Fehrmann, Coll. Surf. A 158 (1999) 255.
[32] O.B. Lapina, V.V. Terskikh, B.S. Bal'zhinimaev, K.M. Eriksen, R. Fehrmann, NATO ASI (2002) 85–104.
[33] O.B. Lapina, V.Yu. Borovkov, G.M. Zhidomirov, L.G. Pinaeva, Kinetika & Katalysis, in press.
[34] A.A. Shubin, O.B. Lapina, V.M. Bondareva, Chem. Phys. Lett. 302 (1999) 341.
[35] O.B. Lapina, A.A. Shubin, A. Nosov, E. Bosch, J. Spengler, H. Knözinger, J. Phys. Chem. 103 (1999) 7599.
[36] O.B. Lapina, D.F. Khabibulin, A.A. Shubin, V.M. Bondareva, J. Mol. Catal. A 162 (2000) 381.
[37] V.V. Terskikh, O.B. Lapina, V.M. Bondareva, Phys. Chem. Chem. Phys. 2 (2000) 2441.